VOL.40 Nº2 2023
https://doi.org/10.22491/rmct.v40i2.11051.en

Estimation of target azimuth based on multiple beamforming processes in a phased array radar system

Vitor Augusto Ferreira Santa Rita[*1], Alberto Gaspar Guimarães[2], Ernesto Leite Pinto[3]
[1]Military Institute of Engineering (IME), Rio de Janeiro (RJ), Brazil, vitoraugusto.rita@ime.eb.br
[2]Universidade Federal Fluminense (UFF), Niterói (RJ), Brazil, agaspar@id.uff.br
[3]Military Institute of Engineering (IME), Rio de Janeiro (RJ), Brazil, ernesto@ime.eb.br

Abstract: *This study investigates the combination of maximum likelihood (ML) with a reduced number of fixed beam steering to estimate target azimuth in a surveillance radar-based system equipped with sensor array. This study describes simulation-based performance results of the estimator using only two fixed beams. It found the great advantage of the ML solution when compared to a usual monopulse estimator, which employs the same number of beams. Additional results show that the investigated ML approach using only one additional beam can obtain greater performance gains.*

Keywords: *Radar. Azimuth Estimation. Antenna Array. Beamforming. Maximum Likelihood.*

Resumo: Investiga-se neste trabalho o emprego de uma abordagem de máxima verossimilhança (ML, de "maximum likelihood") combinada com um número reduzido de conformações de feixe fixas para realizar a estimação do azimute de um alvo num sistema radar de vigilância munido de arranjo de sensores. São apresentados resultados de simulação para avaliação de desempenho do estimador com base em apenas duas conformações. É possível verificar que há grande vantagem do estimador ML em comparação com um estimador monopulso amplamente utilizado que se vale da mesma quantidade de conformações. Resultados adicionais mostram que ganhos maiores de desempenho podem ser obtidos com a abordagem ML aqui investigada utilizando apenas uma conformação de feixe a mais.

Palavras-chave: Radar. Estimação de Azimute. Arranjo de Antenas. Conformação de Feixe. Máxima Verossimilhança.

1. Introduction

The use of antenna array and digital signal processing in radar systems configures an important current resource use that can spatially filter signals, among other operations [1-2]. An important issue in this context refers to estimating the azimuth of a target in relation to radar reference. The literature has several proposals with such aim [3-4].

This study focuses on azimuth estimation in search and surveillance radars [5] that use a linear array of antennas.

Search and surveillance radars generally follow a processing routine in a large volume of space in which:

- the reference direction of the antenna is moved to the center of a sector at each time interval to detect the target and, in case of detection, estimate its position;
- Then, the reference direction to direct the antenna is moved to the center of a neighboring sector to progressively cover the entire region of interest.

Both primary and secondary radars follow this basic routine. The difference for the problem this study addresses refers to the origin of the received signal [5]. In the first case, the signal results from an echo produced by the target in the reference direction in response to a previous transmission from the primary radar. In the second case, the signal is received from a transmission made by a cooperative transmitter (transponder).

In both applications, it is of great interest that the azimuth estimator has great accuracy in the widest possible angular range around the radar reference direction [6-7], which can reduce the total coverage time of the region of interest and thus increase the

update rate of the position information of target [8]. This study will refer to the ability to satisfactorily estimate azimuths around reference directions as the *coverage* of the azimuth estimator.

Another desirable requirement for an azimuth estimator in search and surveillance radars refers to a reduced computational complexity due to the need to repeat its operation at short intervals of time.

A well-known example of a low computational complexity azimuth estimator refers to monopulse techniques [5], originally implemented using two receiving antennas with distinct angular responses. These techniques estimate the azimuth by a linear approximation of the ratio between the difference and the sum of the signals coming from the above-mentioned antennas, called monopulse ratio.

In the case of an azimuth estimator based on a linear array of antennas, an alternative to reduce its complexity refers to using a limited number of fixed beam conformations obtained by appropriate linear combinations of the signals received in the array. The literature on signal processing offers other uses of fixed beam conformations, such as in [9-12].

Overall, two-fixed beam formations can implement a monopulse-type estimator with a linear antenna array, producing very low-complexity solutions. However, monopulse techniques only obtain satisfactory estimations if the target is in a small region close to the antenna reference direction [5,7,13]. In other words, these techniques have small coverage.

Note that, despite the low possibility of detecting a target outside this region, it must still be considered. In such cases, a monopulse technique generates high estimation errors [14], which can be corrected in other processing steps of a radar receiver, but the search for alternatives to avoid or reduce them remains of interest [13].

This study aims to develop and evaluate a more comprehensive estimator using the maximum likelihood technique (ML [15]) using a reduced number of fixed beam formations.

This research first deduces an ML estimator based on multiple beam conformations that address two other unknown parameters in addition to the azimuth. Then, it focuses on azimuth estimation under conditions equal to or close to those usually admitted for the use of monopulse techniques.

The implementation of ML estimators in this research requires a numerical optimization to find the value of the argument that maximizes the objective function. We opted for particle swarm optimization (PSO) [16-18] for this.

This study shows, by simulation results, that the ML approach in a small set of fixed beam conformations can significantly increase the estimation range when compared to a typical monopulse technique.

This study is organized into six sections. Section II describes the model of the adopted system. Section III offers the investigated estimation strategy, section IV shows the equation of the monopulse technique used as reference, and section V describes the results of performance evaluation. Finally, section VI offers the main conclusions of this study.

2. System Model

This study uses an arrangement composed of N_a omnidirectional antenna elements spaced from each other by a fixed distance d along a linear structure. Figure 1 illustrates this type of arrangement.

Fig. 1 - Antenna array model.

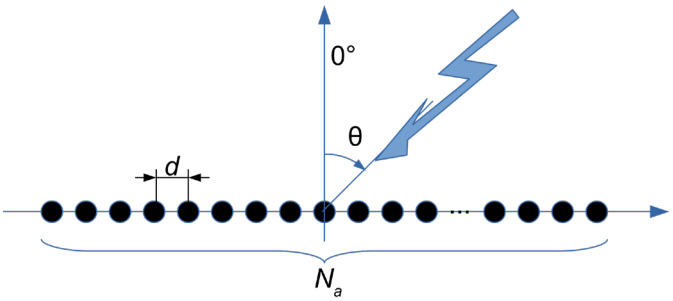

The arrangement enables passive reflection by the target of the signal sent by a primary radar or transmission by a cooperative transmitter with reception of the signal by a secondary radar. Both situations consider that the wavefront from the target falls on the radar at an angle θ with the direction normal to the linear arrangement (Fig. 1).

Considering a scenario with primary radar, the complex envelope of the transmitted signal is given by

$$\tilde{s}_t(t) = \alpha_t(\theta)\rho(t), \quad t \in \left[0, N_p T\right], \tag{1}$$

in which

$$\rho(t) = \sum_{m=0}^{N_p-1} p(t - mT), \tag{2}$$

in which *Np* refers to the number of sequential pulses; *T*, the time interval between pulses; $p(t)$ the basic transmitted pulse shape; and $\alpha_t(\theta)$ a complex amplitude the modulus of which is related to the transmission power in the direction θ.

The baseband equivalent of the signal received by the *k*-th sensor array can be expressed as [11]

$$x_k(t) = \alpha_r(\theta)\rho\left(t - \tau - \frac{kd}{c} sen\theta\right) e^{-j2\pi\left(f_c\tau + k\frac{d}{\lambda} sen\theta\right)} + z_k(t), \tag{3}$$

with $k \in \{0, \cdots, N_a - 1\}$. The terms f_c and λ denote, respectively, the frequency and wavelength of the carrier, *c* is the speed of light and τ is the delay in relation to the moment of transmission.

The breadth of $\alpha_t(\theta)$ depends on the strength from the target (by self-transmission or reflection, depending on the type of radar) and the gain of the reception diagram in θ. This study takes $\alpha_t(\theta)$ as unknown, but not random in nature.

In turn, $z_k(t)$ represents the thermal noise from the *k*-th sensor, which is modeled as a complex Gaussian process with a zero mean and constant power spectral density in a much larger frequency range than that occupied by the signal of interest. Equation (3) ignores a possible Doppler shift of the signal frequency — although this assumption is reasonable for many applications [19].

This study assumes[1] that $N_a d / c \ll \tau$, redefining the complex amplitude by incorporating lag factors that are independent of the position of the sensor. Thus, expression (3) is rewritten as

$$x_k(t) \approx \alpha\rho(t - \tau) e^{-j2\pi\left(k - \frac{N_a - 1}{2}\right)\frac{d}{\lambda} sen\theta} + z_k(t), \tag{4}$$

in which: $\alpha = \alpha_r(\theta) e^{-j\pi\left(2 f_c \tau + (N_a - 1)\frac{d}{\lambda} sen\theta\right)}$.

It is important to note that α depends on θ and τ. However, the problem defined here will disregard dependence, as in [19,20].

Rewriting (4) in vector notation, we have

$$x(t) = \alpha\rho(t - \tau) a(\psi) + z(t), \tag{5}$$

in which $\boldsymbol{x}(t) = \left[x_k(t)\right]_{k=0}^{N_a-1}$ and $\boldsymbol{z}(t) = \left[z_k(t)\right]_{k=0}^{N_a-1}$ configure dimension column vectors N_a x1 and $\boldsymbol{a}(\psi)$, the *vector director*, given by

$$\boldsymbol{a}(\psi) = \left[e^{j\left(\frac{N_a-1}{2}\right)\psi} \quad e^{-j\left(\frac{N_a-1}{2}\right)\psi}\right]^{\mathrm{T}}, \tag{6}$$

in which

$$\psi = 2\pi \frac{d}{\lambda} sen\theta \tag{7}$$

with, $\theta \in \left[-\pi/2, \pi/2\right]$

The signals generated at the output of the sensors ar applied as a set of N_c fixed bundle forming, as shown in Figure 2, which illustrates the sequence of the main operations performed on the receiver.

The signals generated by the conformations are given by

$$y(t) = W^H x(t) \; y(t) = W^H x(t) \tag{8}$$

$$= \alpha\rho(t - \tau) g(\psi) + v(t), \tag{9}$$

1 A valid assumption since the distance from the radar to the target is usually much greater than $N_a d$.

in which

$$g(\psi) = W^{H} a(\psi), \qquad (10)$$

$$v(t) = W^{H} z(t) \qquad (11)$$

and W is the fixed forming matrix with $N_a \times N_c$. dimensions. Each column of this matrix corresponds to the normalized beamforming vector in a given direction $\theta_c \in [-\pi/2, \pi/2]$, defined as

$$w_{\psi_c} \underline{\underline{def}} \frac{1}{\sqrt{N_a}} a(\psi_c), \qquad (12)$$

with $c \in \{1, \cdots, N_c\}$, $a(.)$ defined in Equation (6) and $\psi_c = 2\pi \frac{d}{\lambda} sen\theta_c$.

Fig. 2 - Receiver block diagram.

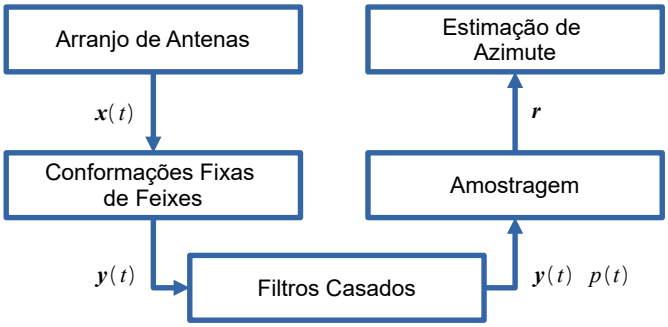

Note that if W unitary, i.e., $WW^{H} = I$, the noise vector $v(t)$ has the covariance matrix $E[v(t)v^{H}(t)] = \sigma^2 I$. [15] has shown that this condition is achieved if $\theta_{c_i} - \theta_{c_j} = 2k\pi / N_a$, $\forall c_i, c_j \in \{0, \ldots, N_c - 1\}$ and $k \in Z$.

As Figure 2 shows, the signals resulting from the beam conformations pass through matched filters and are sampled, giving rise to the input of the azimuth estimator. The sampling times given by

$$t_{l,m} = t_0 + (l-1)T_a + (m-1)T, \qquad (13)$$

toward $m \in \{1, \ldots, N_p\}$ and $l \in \{1, \ldots, L\}$ in which L is the number of successive samples per pulse and T_a, the time interval between samples.

This study takes that the pulse at the outlet of the matched filter has significant energy in the range of T_p seconds and that the initial instant T_0 is such that

$$t_0 \in [\tau - T_p/2; \tau + T_p/2]. \qquad (14)$$

Figure 3 shows an example in which the pulse at the outlet of the matched filter is triangular.

Figure 3 - Example of sampling instants.

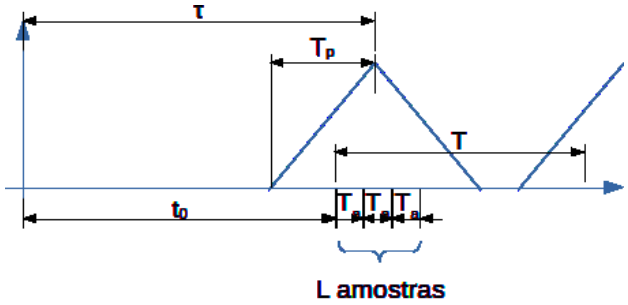

The $N_p L$ samples obtained for each beam conformation are assembled in the vector r dimension $(N_c L N_p) \times 1$ given by

$$r = \alpha n(\psi, \tau) +, \qquad (15)$$

in which

$$\varsigma(\psi, \tau) = \begin{bmatrix} g_1(\psi) \div_\tau \\ g_2(\psi) \div_\tau \\ \vdots \\ g_{N_c}(\psi) \div_\tau \end{bmatrix}, \qquad (16)$$

in which $g_c(\psi)$ is the c-th element of the vector $g(\psi)$ in Equation (10) and χ_τ is a vector with a $(LN_p) \times 1$ dimension with samples from the square wave resulting from the filtering of $\rho(t - \tau)$ obtained at moments $t_{l\,m}$.

Still in expression (15), the noise vector n it is Gaussian with a null mean, which can be expressed as

$$n = [n_1 \quad \cdots \quad n_{N_c}]^T, \qquad (17)$$

In which n_c is the column vector that gathers the samples of the filtered noise associated with the c-th conformation.

Therefore, from (15), the vector of observations r Gaussian with the following vector mean

$$\mu = E[r] = \alpha\eta(\psi,\tau) \qquad (18)$$

and the following covariance matrix

$$\Sigma = E\left[(r-\mu)(r-\mu)^{\mathrm{H}}\right] = E\left[nn^{\mathrm{H}}\right], \qquad (19)$$

which can be expressed in blocks such as

$$\Sigma = \begin{bmatrix} \Sigma_{c_1c_1} & \cdots & \Sigma_{c_1c_{N_c}} \\ \vdots & \ddots & \vdots \\ \Sigma_{c_{N_c}c_1} & \cdots & \Sigma_{c_{N_c}c_{N_c}} \end{bmatrix}, \qquad (20)$$

in which $\Sigma_{c_ic_j} = \mathrm{E}\left[n_{c_i}n_{c_j}^{\mathrm{H}}\right]$ with $c_i, c_j \in \{1,\cdots,N_c\}$.

3. ML Estimation

The vector of observations r in Equation (15) is Gaussian, with only the mean vector dependent on the parameters (α,τ,ψ). Therefore, the logarithmic likelihood function [15] can be expressed as

$$l\left((\alpha,\tau,\psi);r\right) =$$

$$\frac{-1}{2}\left(r-\alpha\eta(\psi,\tau)\right)^H \Sigma^{-1}\left(r-\alpha\eta(\psi,\tau)\right)+\xi, \qquad (21)$$

in which ξ is a scalar constant that dispenses with the parameters α,τ and ψ. The maximum likelihood estimate [15] of these parameters is the argument that maximizes $l(\cdot)$ or, equivalently,

$$\left(\hat{\alpha}_{ML}(r),\hat{\tau}_{ML}(r),\hat{\psi}_{ML}(r)\right) = \underset{(\alpha,\tau,\psi)}{argmin}\ \nu(\alpha,\tau,\psi;r), \qquad (22)$$

in which

$$\nu(\alpha,\tau,\psi;r) = \left(r-\alpha\eta(\psi,\tau)\right)^{\mathrm{H}} \Sigma^{-1}\left(r-\alpha\eta(\psi,\tau)\right). \qquad (23)$$

The estimate $\hat{\alpha}_{ML}(r)$ can be obtained from the equation below, which establishes a necessary condition for minimizing $\nu(\cdot)$, depending on the parameter α:

$$\left.\frac{\partial\nu}{\partial\alpha}\right|_{\alpha=\hat{\alpha}_{ML}} = 0. \qquad (24)$$

After some algebraic manipulations, considering that Σ dispenses with α, we arrive at

$$\hat{\alpha}_{ML}(r) = \frac{\boldsymbol{\varsigma}^H(\psi,\tau)\boldsymbol{\acute{O}}^{-1}\boldsymbol{r}}{\boldsymbol{\varsigma}^H(\psi,\tau)\boldsymbol{\acute{O}}^{-1}\boldsymbol{\varsigma}(\psi,\tau)}. \qquad (25)$$

With the above result, the strategy adopted to determine the ML estimate of (τ,ψ) refers to replacing Equation (25) in Equation (23), obtaining, after a few steps, the following solution:

$$\left(\hat{\tau}_{ML}(r),\hat{\psi}_{ML}(r)\right) = \underset{(\tau,\psi)}{argmax}\frac{\left|\boldsymbol{\varsigma}^H(\psi,\tau)\boldsymbol{\acute{O}}^{-1}\boldsymbol{r}\right|^2}{\boldsymbol{\varsigma}^H(\psi,\tau)\boldsymbol{\acute{O}}^{-1}\boldsymbol{\varsigma}(\psi,\tau)}, \qquad (26)$$

which requires the implementation of numerical optimization.

Once the estimates of $\left(\hat{\tau}_{ML}(r),\hat{\psi}_{ML}(r)\right)$, we return to Equation (25) to obtain $\hat{\alpha}_{ML}(r)$.

3.1 Unit conformation matrix

If the matrix W of conformation is unitary, it is easy to find that $\Sigma_{c_ic_j} = 0$ (null array) to $i \neq j$. This shows, based on the expression in Equation (20), that Σ configures a diagonal block matrix.

Thus, the ML estimates of the parameters of interest are given by

$$\left(\hat{\tau}_{ML}(r),\hat{\psi}_{ML}(r)\right) = \underset{(\tau,\psi)}{argmax}\frac{\left|\sum_{c=1}^{N_c} g_c(\psi)\chi_\tau^{\mathrm{H}}\Sigma_{cc}^{-1}r_c\right|^2}{\sum_{c=1}^{N_c}\left|g_c(\psi)\right|^2\chi_\tau^H\Sigma_{cc}^{-1}\chi_\tau} \qquad (27)$$

and

$$\hat{\alpha}_{ML}(r) = \left.\frac{\sum_{c=1}^{N_c} g_c(\psi)\chi_\tau^{\mathrm{H}}\Sigma_{cc}^{-1}r_c}{\sum_{c=1}^{N_c}\left|g_c(\psi)\right|^2\chi_\tau^{\mathrm{H}}\Sigma_{cc}^{-1}\chi_\tau}\right|_{\substack{\tau=\hat{\tau}_{ML}(r)\\ \psi=\hat{\psi}_{ML}(r)}}, \qquad (28)$$

in which r_c the vector of observations obtained for the c-conformation.

Note that the vectors and matrices in Equation (27) have dimensions N_c times smaller than in Equation (26), making the optimization procedure computationally much simpler.

3.2 Numerical optimization

We chose to use the PSO technique to numerically obtain the azimuth and delay estimates in equations (26) and (27).

The original PSO algorithm was described in [17]. It uses a swarm formed by a set of particles that evolves over iterations to perform a very flexible scan of the search space for the optimal value of the objective function. Use cases of the PSO algorithm in ML parameter estimation have been described, for example, in [16,18,21]. This study chose the version of this algorithm called Accelerated Particle Swarm Optimization (APSO), which shows rapid convergence [22].

4. Monopulse technique

Monopulse-type techniques [5] based on a linear array of sensors simultaneously generate two values resulting from beam conformations (Figure 4). Calculating the ratio between the difference and the sum of these values obtains the monopulse ratio, which is used to achieve the azimuth estimate.

Fig. 4 - Azimuth estimation by monopulse radar with sensor array.

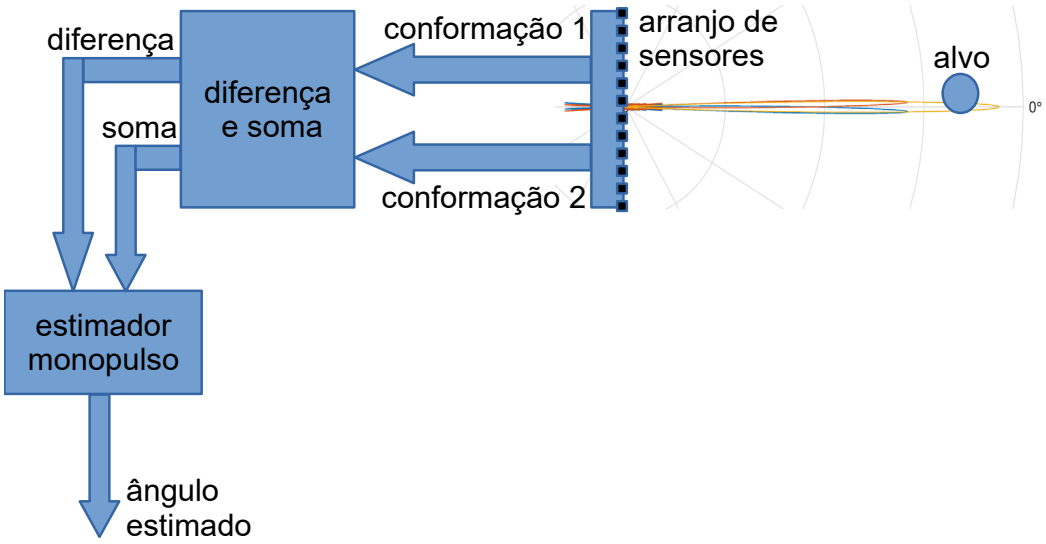

4.1 Monopulse amplitude

The specific case of the monopulse amplitude technique define the two beam formations with symmetrical inclinations in relation to the direction normal to the linear arrangement. $w_{\psi_{+\delta}}$ and $w_{\psi_{-\delta}}$ refer to the used conformation vectors, corresponding respectively, to the $\psi_{+\delta}$ and $_{-\delta}$ slopes, which are expressed according to equation (12).

Moreover, after filtration, the signals from these conformations are sampled at instant $t = t_0 = \tau$, obtaining, based on equations (15) and (16), the vector given by

$$r = \begin{bmatrix} \alpha\chi_1 w_{\psi_{+\delta}}^{\mathrm{H}} a(\psi) + n_{\psi_{+\delta}} \\ \alpha\chi_1 w_{\psi_{-\delta}}^{\mathrm{H}} a(\psi) + n_{\psi_{-\delta}} \end{bmatrix}. , \qquad (29)$$

In which $n_{\psi_{+\delta}}$ and $n_{\psi_{-\delta}}$ are noise samples associated with the respective conformations.

The monopulse ratio consists of

$$\beta \overset{def}{=\!=} \frac{r_1 - r_2}{r_1 + r_2}, \qquad (30)$$

in which r_1 and r_2 are the first and second elements of r in the Equation (29) , respectively.

The idealized monopulse ratio disregards the noise portions in Equation (30), given by

$$\beta_{id}(\psi) \overset{def}{=\!=} \frac{\left(\boldsymbol{w}_{\psi_{+\delta}}^{\mathrm{H}} - \boldsymbol{w}_{\psi_{-\delta}}^{\mathrm{H}}\right)\boldsymbol{a}(\psi)}{\left(\boldsymbol{w}_{\psi_{+\delta}}^{\mathrm{H}} + \boldsymbol{w}_{\psi_{-\delta}}^{\mathrm{H}}\right)\boldsymbol{a}(\psi)}. \qquad (31)$$

Substituting equations (12) and (6) into the previous equation and assuming an odd N_a2 obtains, after some algebraic manipulations,

$$\beta_{id}(\psi) = \frac{\sum_{k=1}^{(N_a-1)(N_a-1)/2} sen(k\psi)\, sen(k\psi\ )}{1/2 + \sum_{k=1}^{(N_a-1)(N_a-1)/2} cos(k\psi)\, cos(k\psi\ )}. \qquad (32)$$

The linear approximation of $\beta_{id}(\psi)$ around $=0$ is given by

$$\beta_{id}(\psi) \approx \beta_{id}^{'}(0)\psi, \qquad (33)$$

in which $\beta_{id}^{'}(0)$ is the derivative of $\beta_{id}(\psi)$ in $\psi = 0$, which can be calculated by the expression

$$\beta_{id}^{'}(0) = \frac{\sum_{k=1}^{(N_a-1)(N_a-1)/2} ksen(k\psi_{\delta})}{1/2 + \sum_{k=1}^{(N_a-1)(N_a-1)/2} cos(k\psi_{\delta})}. \qquad (34)$$

Assuming that the real part of the measured monopulse ratio in Equation (30) can be approximated by $\beta_{id}(\psi)$ and that this can be approximated by (33), we finally arrive at the following expression for the estimate of ψ. Using this monopulse amplitude technique:

2 The development considering N_a pair is quite similar.

Fig. 5 - Illustration of the evolution of four swarm particles in the implementation of the ML(2) estimator with SNR = 20 dB and target azimuth at 0 rad.

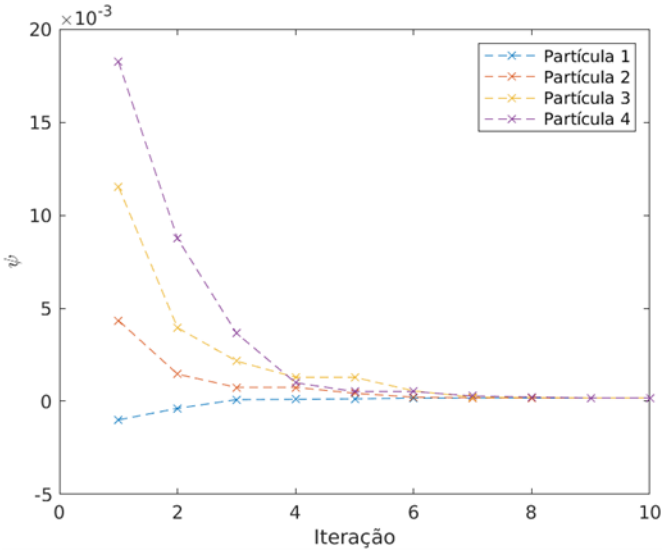

$$\hat{\psi}_{mp} = \frac{\Re e[\beta]}{\beta_{id}^{'}(0)}, \qquad (35)$$

In which $\Re e[.]$ denotes the actual part of the argument and $\beta_{id}^{'}(0)$, a constant calculated using equation (34).

5. Performance Assessment

This study carried out simulations of a radar receiver with a radar array, with $N_a = 101$ elements spaced $d = \lambda/2$ apart and a signal with a basic rectangular pulse.

The considered signal-to-noise ratio (SNR) is given by dividing the average power of the signal of interest at the input of the array by the average noise power in the frequency range occupied by this signal. For this, the bandwidth was considered the inverse of the duration of the basic pulse.

The comparison with amplitude monopulse only considered two conformations ($N_c = 2$) in the use of the ML technique.

In the following text, ML(N_c) denotes the ML estimation technique with N_c conformations and MA, the monopulse amplitude estimator above.

This comparison assumes the delay parameter (τ) is known, which is usually done in studies addressing monopulse techniques [5,6,7,14].

In more specific terms, ML estimates were obtained as a solution to the optimization problem in ψ with the objective function given by equation (26), assuming the known value of τ . It is worth remembering that ψ has a one-to-one relation with the physical angle of arrival of the signal at the input of the array in Equation (7).

Regarding the APSO algorithm, the number of used particles totaled 30 and the number of iterations until the stop was empirically adjusted and totaled 15.

Figure 5 illustrates the evolution over iterations of the four-particle azimuth estimate cluster by the APSO algorithm, which was obtained with SNR = 20 dB and target azimuth at 0 rad.

In Figure 5 shows that, from the eighth iteration onward, a significant concentration of estimates occur around the real value of the target angle.

On the other hand, Figure 6 shows three examples of the evolution of estimation error obtained with a swarm of 30 particles and 30-, 20-, and 10-dB SNRs.

A rapid stabilization of the error and coherence between SSR and error occur, in the sense that the increase in the former is associated with the reduction of the latter. Other tests of this type have observed similar behaviors.

Figure 6 - Estimation error with the ML(2) technique and different RSR values.

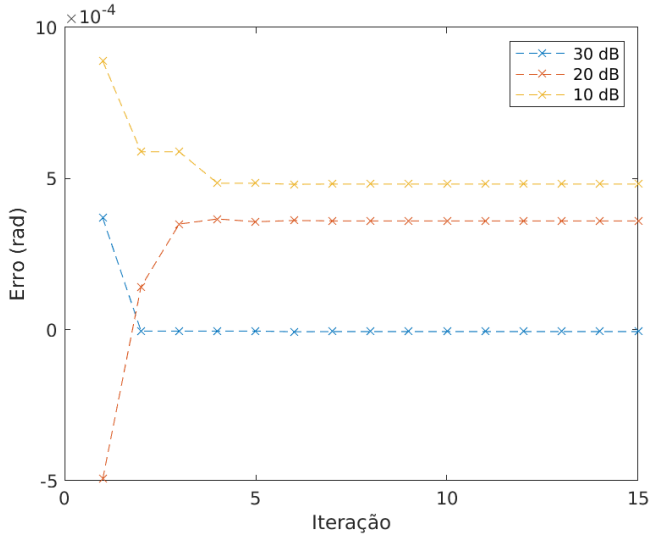

This study now describes the results of empirical evaluation of polarization, variance, and mean square error (MSE) of different estimators, obtained based on 2,000 independent achievements.

A first performance comparison between the ML(2) and MA techniques was performed with slopes $\psi_{\pm\delta} = \pm 0,028$ Rad. Figure 7 shows the results obtained with a 10-dB of SNR.

This figure evinces that the performance of the MA estimator is practically identical to that of the ML(2) estimator for low values of target azimuth, with very significant differences for higher values, especially the growth of the polarization of the monopulse estimator above 0.04 rad. It is also noticed that the performance degradation of this estimator increases to higher azimuth values, so the MSE increases rapidly.

These performance characteristics of the MA estimator can, to a large extent, be seen as a direct consequence of the inaccuracy in the linear approximation of the monopulse ratio, which increases with greater azimuth values. Figure 8 illustrates this effect for the idealized monopulse ratio corresponding to the conditions in Figure 7.

Figure 7 - Performance of ML(2) and MA estimators as a function of target azimuth with a 10-dB SNR.

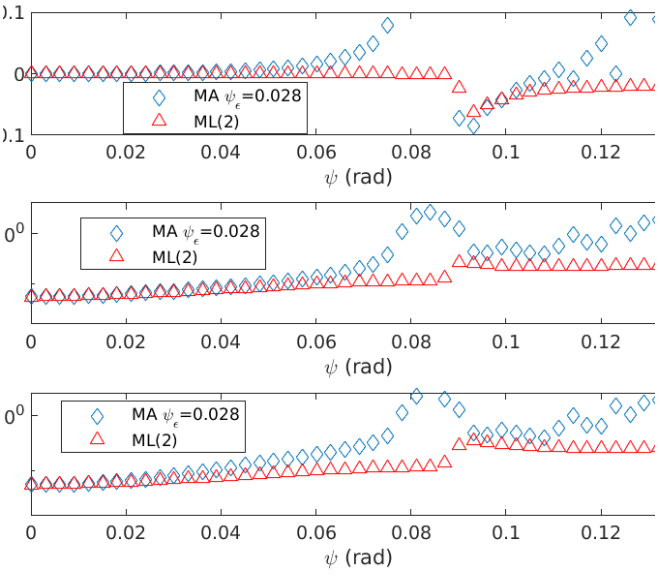

Figure 8 shows that, in fact, the linear approximation is satisfactory for azimuth values slightly below 0.04 rad and becomes generally inadequate with azimuths above this value.

Figure 8 - Idealized MA ratio and its linear approximation as a function of the target azimuth.

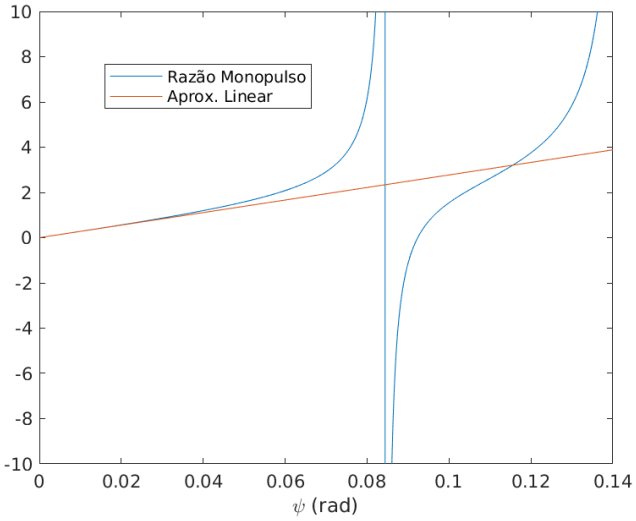

Regarding the ML(2) estimator, Figure 7 shows it has practically negligible polarization for azimuth values up to about 0.09 rad.

The results of this figure show, as a whole, that the ML(2) estimator has a significantly higher overall performance than the MA estimator for azimuth values from 0.04 to 0.09 rad, significantly increasing *coverage*.

Figure 9 results were obtained with an SNR of 20 dB and the same slopes $\psi_{\pm o} = \pm 0,028$ Rad. These results confirm the increase in *coverage* from the ML(2) estimator when compared to MA. In particular, results are practically identical to those of Figure 7 regarding polarization comparison.

This research performed a more detailed analysis of the objective function of the ML(2) estimator was performed and found that the increase in the azimuth of the target can lead to the frequent occurrence of two local minima of this function, as illustrated in the example in Figure 10.

In this figure, the objective function the ML(2) estimator used shows two very close minimum values, associated with values that quite differ from its argument, one of which corresponds to the correct azimuth of the target. Situations similar to this can lead to high estimation errors and consequent increase in the MSE.

Figure 9 - Performance of ML(2) and MA estimators as a function of target azimuth with a 20-dB SNR.

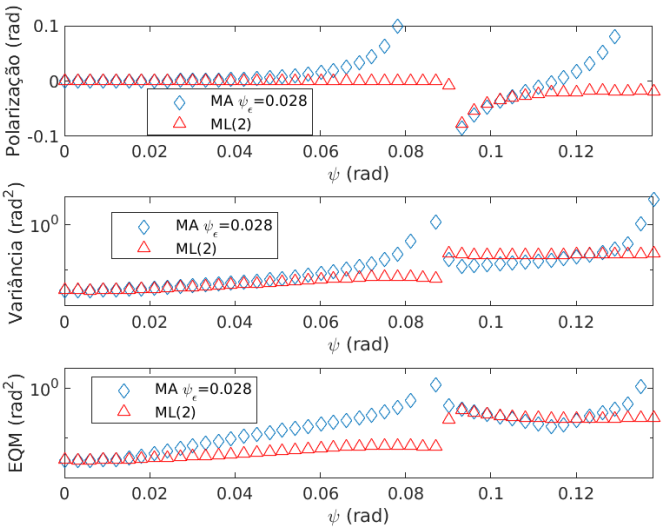

However, this study found that the increase in the number of used conformations reduces the intensity of this problem. The results below illustrate this finding.

Fig. 10 - Example of an objective function used by the ML(2) estimator, obtained with a 0.10-rad target azimuth and a 20-dB SNR.

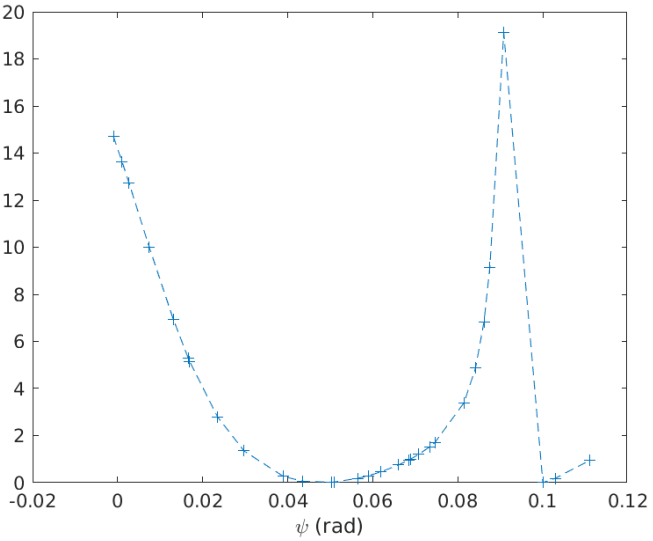

5.2 Increase in the number of formations

To implement the ML(3) estimator, a conformation with a $\psi_0 = 0$ rad slope and two conformations with $\psi_{\pm 0} = \pm 0{,}056$ Rad slopes were used. The used conformations with the ML(2) were the same as those above.

The Figure 11 shows the performance results obtained with these estimators for an SNR of 10 dB.

Fig. 11 - Performance of the ML(2) and ML(3) estimators as a function of the target azimuth with a 10-dB SNR.

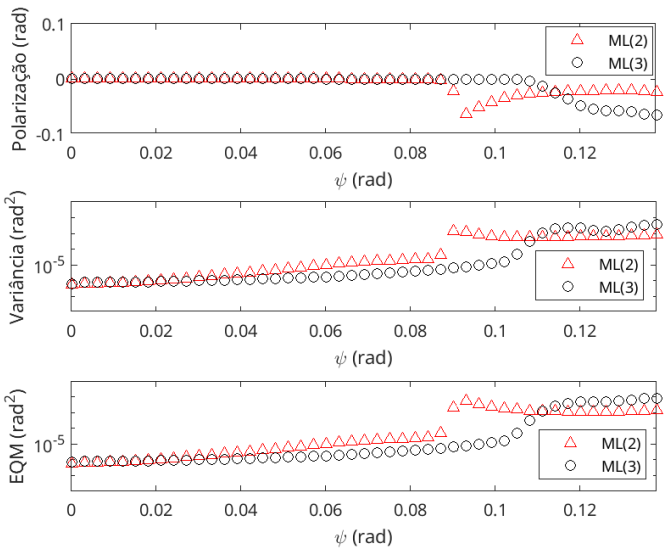

The use of three conformations can improve estimation *coverage*, providing an MSE that remains fundamentally stable up to azimuth values of the order of 0.105 rad, which represents an increase of about 20% over the *coverage* of the ML estimator(2).

Figure 12 shows the performance results of the same estimators obtained with a 20-dB SNR. This figure shows an improvement due to the increase in the SNR and that the ML(3) estimator increases coverage by around 20%.

Other simulations show ML estimations can obtain even greater gains of *coverage* if combined with the use of more than three conformations.

Fig. 12 - Performance of the ML(2) and ML(3) estimators as a function of the target azimuth with a 20-dB SNR.

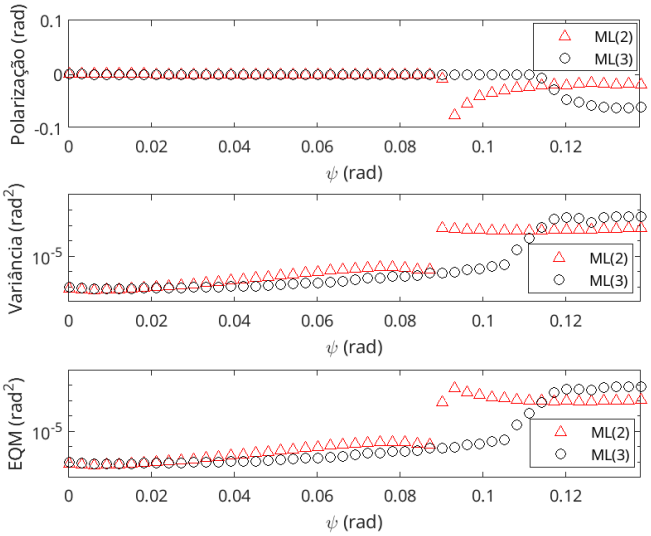

5.3 Computational complexity

The investigated ML estimators performed better than the MA estimator but have higher complexity, mainly due to the need to implement numerical optimization.

However, it should be noted that there remains room for research for algorithms for this implementation with reduced computational cost. This study implemented with APSO [22] but other alternatives exist and may be tried in future researches, for example, combining techniques — as suggested in [14] — or using approximate objective functions (in relation to the original objective function), reducing the computational costs of optimization.

Conclusions

This study investigated the use of maximum likelihood (ML) to estimate the azimuth of a target in radar systems with sensor array. The considered receiver model subjects the set of signals at the output of the array to fixed beam conformations, followed by filtering and sampling steps, to generate the vector of observations to estimate angles.

This study first evaluated an ML estimator that can produce delay parameters and obtain complex amplitude of the received signal. Then, it investigated the performance of a simplified version of this estimator, aimed only at obtaining the azimuth, using two beam conformations. Compared to the alternative, which uses the monopulse technique, the evaluated ML azimuth estimator provides accurate estimates at longer intervals but has a higher computational cost as it requires numerical optimization to obtain its estimates.

This research also evaluated the effect of a small increase in the number of input conformations in the ML to estimate the azimuth and found that an additional conformation improves the initially verified performance advantages.

Directions for the continuation of this investigation in future works were pointed out, especially aiming at reducing the computational complexity of ML estimators. Still in the perspective of continuing this research, it should be noted that, assuming the use of a two-dimensional array of sensors, the ML solution considered here can easily be extended to encompass the target elevation angle. The investigation of the performance of the position estimator thus obtained also offers an alternative for future studies.

References

[1] MAILLOUX, R. J. *Phased array antenna handbook*. [S. l.]: Artech House, 2017.
[2] RICHARDS, M.; SCHEER, J.; HOML, W. *Principles of Modern Radar: Basic Principles*. London: Institution of Engineering and Technology, 2010.
[3] XU, J.; WANG, W. Q.; GUI, R. Computational Efficient DOA, DOD, and Doppler Estimation Algorithm for MIMO Radar. *IEEE Signal Processing Letters*, [*s. l.*], v. 26, n. 1, p. 44-48, 2019.
[4] CHAHROUR, H.; DANSEREAU, R.; RAJAN, S.; BALAJI, B. Direction of Arrival Estimation using Riemannian Mean and Distance. *IEEE Radar Conference*, Boston, p. *1-5, 2019*1-5, 2019.
[5] SHERMAN, S.; BARTON, D. *Monopulse Radar Theory and Practice*. [S. l.]: Artech House, 2011.
[6] JAIN, V.; EHRMAN, L. M.; BLAIR, W. D. Estimating the DOA mean and variance of off-boresight targets using monopulse radar. *IEEE Proceeding of the Thirty-Eighth Southeastern Symposium on System Theory*, [*s. l.*], p. 85-88, 2006.
[7] SHARENSON, S. Angle estimation accuracy with a monopulse radar in the search mode. *IRE Transactions on Aerospace and Navigational Electronics*, [*s. l.*], n. 3, p. 175-179, 1962.
[8] GROSSI, E.; LOPS, M.; VENTURINO, L. A search-and-revisit scanning policy to improve the detection rate in agile-beam radars. *IEEE Workshop on Statistical Signal Processing (SSP)*, [*s. l.*], p. 452-455, 2014.
[9] GORWARA, A.; MOLCHANOV, P. Multibeam monopulse radar for airborne sense and avoid system. *SPIE Unmanned/Unattended Sensors and Sensor Networks XII*, [*s. l.*], v. 9986, p. 9-22, 2016.
[10] DAI, H.; HAN, H.; WANG, J.; XU, X.; QIAO, H. An improved high angular resolution method by using four--channel jointed monopulse radar. *In*: IEEE Progress Electromagnetics Research Symposium-Spring (PIERS), [*s. l.*], p. 3056-3061, 2017.
[11] TREES, H. V. *Optimum Array Processing*: Part IV of Detection, Estimation, and Modulation Theory. London: Wiley, 2004.
[12] CHANG, D.; ZHENG, B. Adaptive generalized sidelobe canceler beamforming with time-varying direction-of--arrival estimation for arrayed sensors. *IEEE Sensors Journal*, [*s. l.*], v. 20, n. 8, p. 4403-4412, 2019.
[13] DAVIS, R.; FANTE, R. A maximum-likelihood beamspace processor for improved search and track. *IEEE Transactions on Antennas and Propagation*, [*s. l.*], v. 49, n. 7, p. 1043-1053, 2001.
[14] Nickel, U. Overview of generalized monopulse estimation. *IEEE Aerospace and Electronic Systems Magazine*, [*s. l.*], v. 21, n. 6, p. 27-56, 2006.
[15] Trees, H. V. *Detection, estimation, and modulation theory, part I*: detection, estimation, and linear modulation theory. London: Wiley, 2004.
[16] ÖZSOY, V. S.; ÖRKCÜ, H. H.; BAL, H. Particle swarm optimization applied to parameter estimation of the four-parameter Burr III distribution. *Iranian Journal of Science and Technology, Transactions A: Science*, [*s. l.*], v. 42, n. 2, p. 895-909, 2018.

[17] POLI, R.; KENNEDY, J.; BLACKWELL, T. Particle swarm optimization. *Swarm Intelligence*, [*s. l.*], v. 1, n. 1, p. 33-57, 2007.
[18] NAJJARZADEH, M.; SADJEDI, H. *Implementation of particle swarm optimization algorithm for estimating the innovative parameters of a spike sequence from noisy samples via maximum likelihood method*. Digital Signal Processing. Amsterdam: Elsevier, 2020.
[19] GLASS, J. D.; BLAIR, W. Range estimation using adjacent matched filter samples. *IEEE Aerospace Conference*, [*s. l.*], p. 1-7, 2014.
[20] WANG, J.; WANG, T.; WU, J. Improved target direction-of-arrival estimation using multiple adjacent beams for airborne phased array scanning radar. *IET Radar, Sonar & Navigation*, [*s. l.*], v. 12, n. 2, p. 239-243, 2018.
[21] SCHWAAB, M.; BISCAIA JR, E. C.; MONTEIRO, J. L.; PINTO, J. C. Nonlinear parameter estimation through particle swarm optimization. *Chemical Engineering Science*, [*s. l.*], v. 63, n. 6, p. 1542-1552, 2008.
[22] YANG, X. S. *Particle swarm optimization*. Nature-Inspired Optimization Algorithms. [S. l.]: Academic Press, 2021.
[23] CLERC, M. *Beyond standard particle swarm optimization*. Innovations and Developments of Swarm Intelligence Applications. [*S. l.*]: IGI Global, 201